UNVEILING MOLECULAR INTERACTIONS: COUMARIN DERIVATIVES AND DENGUE VIRUS PROTEIN TARGETS

HEZHA O. RASUL [1], KARZAN R. SIDIQ [2], DIYAR A. HASSAN [3,4], GUILLERMO SALGADO M [5], L. H. MENDOZA-HUIZAR [6], ASSIA BELHASSAN [7], LORENA GERLI CANDIA [8], WILSON CARDONA V [9], AND WILLIAM N. SETZER [10]*

[1]*Department of Pharmaceutical Chemistry, College of Science, Charmo University, Peshawa Street, Chamchamal, 46023, Sulaimani, Iraq.*
[2]*Department of Medical Laboratory Science, College of Science, Charmo University, Peshawa Street, Chamchamal, 46023, Sulaimani, Iraq.*
[3]*Bright Technical and Vocational Institute, Department of Pharmacy, Sulaymaniyah, Kurdistan Region, Iraq.*
[4]*Pioneer Company for Pharmaceutical Industries, Quality Control Department, Sulaymaniyah, Kurdistan Region, Iraq.*
[5]*Facultad de Ciencias Químicas. Investigador Extramural, Universidad de Concepcion, Concepcion, Chile.*
[6]*Autonomous University of Hidalgo State. Academic Area of Chemistry. Mineral de la Reforma, Hidalgo. México.*
[7]*Molecular Chemistry and Natural Substances Laboratory, Faculty of Science, Moulay Ismail University of Meknes, Morocco.*
[8]*Departamento de Química Ambiental, Facultad de Ciencias, Universidad Católica de la Santísima Concepción, Concepción, Chile.*
[9]*Facultad de Medicina y Ciencia, Universidad San Sebastian, Puerto Montt, Chile.*
[10]*Department of Chemistry, University of Alabama in Huntsville, Huntsville, AL 35899, USA.*

ABSTRACT

Dengue virus (DENV) remains a significant global health threat, with its transmission spanning across a minimum of 128 countries. This viral disease puts nearly 4 billion people at risk worldwide, so the exploration of innovative therapeutic strategies is necessary [1–5]. Dengue fever is a Flaviviral infection transmitted by mosquitoes, predominantly by *Aedes aegypti*, and to a lesser extent by *Aedes albopictus* and other *Aedes* species [4,6]. The dengue virus is an enveloped spherical virus, possessing a single stranded RNA genome. It also has three structural proteins, including, the capsid (C), membrane (M) and envelope (E), and seven non-structural proteins, including NS1, NS2A, NS2B, NS3, NS4A, NS4B and NS5. These nonestructural proteins play various roles in viral replication [7–9] **(Figure 1)**. The dengue virus is categorized into five distinct serotypes—DENV-1, DENV-2, DENV-3, DENV-4, and DENV-5 based on antigenic variability. All serogroups cause severe and critical health issues [8,10,11]. The incubation period for dengue fever spans 4–7 days. The spectrum of the disease encompasses asymptomatic infection and mild febrile illness (referred to as dengue fever) to more severe manifestations, including dengue hemorrhagic fever (DHF) and dengue shock syndrome (DSS) [12]. The most critical syndrome may present as dengue shock syndrome (DSS), characterized by coagulation abnormalities, plasma leakage, and heightened vascular fragility. The loss of fluids due to increased capillary permeability results in hypovolemic shock and multi-organ failure [13]. Annually, around 20,000 deaths occur due to dengue virus infection, particularly in cases associated with secondary dengue and DHF/DSS.

Keywords: Dengue Virus, Envelope Glycoprotein, Molecular Docking, ADMET, Molecular Dynamic.

INTRODUCTION

Dengue virus (DENV) remains a significant global health threat, with its transmission spanning across a minimum of 128 countries. This viral disease puts nearly 4 billion people at risk worldwide, so the exploration of innovative therapeutic strategies is necessary [1–5]. Dengue fever is a Flaviviral infection transmitted by mosquitoes, predominantly by *Aedes aegypti*, and to a lesser extent by *Aedes albopictus* and other *Aedes* species [4,6]. The dengue virus is an enveloped spherical virus, possessing a single stranded RNA genome. It also has three structural proteins, including, the capsid (C), membrane (M) and envelope (E), and seven non-structural proteins, including NS1, NS2A, NS2B, NS3, NS4A, NS4B and NS5. These nonestructural proteins play various roles in viral replication [7–9] **(Figure 1)**. The dengue virus is categorized into five distinct serotypes—DENV-1, DENV-2, DENV-3, DENV-4, and DENV-5 based on antigenic variability. All serogroups cause severe and critical health issues [8,10,11]. The incubation period for dengue fever spans 4–7 days. The spectrum of the disease encompasses asymptomatic infection and mild febrile illness (referred to as dengue fever) to more severe manifestations, including dengue hemorrhagic fever (DHF) and dengue shock syndrome (DSS) [12]. The most critical syndrome may present as dengue shock syndrome (DSS), characterized by coagulation abnormalities, plasma leakage, and heightened vascular fragility. The loss of fluids due to increased capillary permeability results in hypovolemic shock and multi-organ failure [13]. Annually, around 20,000 deaths occur due to dengue virus infection, particularly in cases associated with secondary dengue and DHF/DSS.

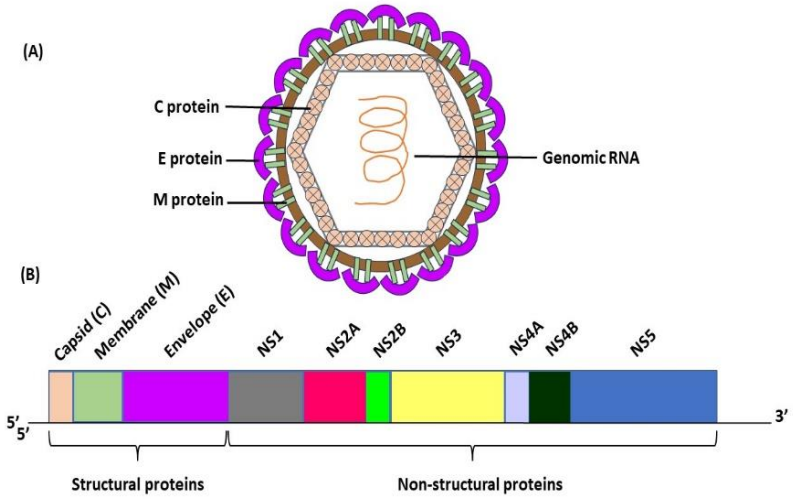

Figure 1: The structure of Dengue virus (A) and its proteins expressed loci on the virus genomic RNA (B)

**Corresponding author email: hezha.rasul@chu.edu.iq*

Coumarin is a naturally produced secondary metabolite and has been identified as a therapeutic substance. Coumarin is isolated from various sources, such as plants, fungi, bacteria, and essential oils, and can also be artificially created [14]. Coumarins have been discovered in diverse plant families, including *Rutaceae, Umbelliferae, and Clusiaceae* [15]. The isolation of coumarin from Tonka beans occurred independently in 1820, with A. Vogel from Munich, Germany, and Nicholas Guibourt from France both contributing to its discovery [16]. The first synthesis of coumarin was accomplished in 1868 by the English chemist, William Henry Perkin [17]. Benzene and benzopyrene (an alpha-pyrene ring) are fused to form the basic building blocks of coumarin [14]. Numerous synthetic pathways, such as the Pechmann reaction, Knoevenagel condensation, metal-catalyzed cyclization, and Perkin condensation, can be used to create derivatives of coumarin [3,18]. Coumarins are characterized by stability, solubility, and a low molecular weight, devoid of any detrimental side effects or toxicity. These features, along with several others, position coumarins as potential candidates for drug development against numerous viral and bacterial diseases. Various lead compounds with a coumarin scaffold, derived from natural, synthetic, conjugated, and hybrid sources, have undergone study and are advancing through different phases of drug development [19]. The biological activity of these compounds can be modulated based on the combination of different substituents and conjugates. Furthermore, coumarin motifs can be anticipated as a favored framework and foundational structure for creating and synthesizing various pharmacological compounds with notable binding affinity for diverse biological targets. Their adaptability allows for easy modifications to meet Lipinski's "rule of 5," transforming them into drug-like molecules through a privileged structure approach in drug discovery by employing combinatorial chemistry [20]. The thorough investigations into coumarin's efficacy as an antiviral compound, specifically against Influenza, HIV, coxsackievirus A16, and Enterovirus 71 [3,21–25], along with its therapeutic applications, have sparked the curiosity of scientists to further explore its potential in combatting and managing various viral illnesses [26].

Molecular docking studies have become indispensable tools in drug discovery, allowing researchers to predict and analyze the binding interactions between ligands and target proteins at the molecular level. In this context, the present research endeavors to unravel the intricate molecular interactions between coumarin derivatives and the key Dengue virus protein targets through advanced computational techniques. The convergence of molecular docking studies, molecular dynamics (MD) simulations, binding free energy calculations using Molecular Mechanics-Generalized Born Surface Area (MM-GBSA), and predictive analyses such as Lipinski's Rule and absorption, distribution, metabolism, and excretion–toxicity (ADMET) prediction hopefully offer a comprehensive understanding of the potential therapeutic efficacy of coumarin derivatives against Dengue virus [27,28].

MATERIALS AND METHODS

Molecular Docking Studies

Protein-ligand docking studies were carried out using Molegro Virtual Docker (Version 6.0.1, Molegro ApS, Aarhus, Denmark) [29] of the coumarin ligands with structures of dengue virus potential protein targets: C-terminal NS3; helicase (PDB ID: 2BHR, 2BMF, 2JLQ, 2JLR, 2JLS, 2JLU, 2JLV, 2JLX, 2WHX, and 5XC6) [30–33], N-terminal NS5; RNA methyl transferase (PDB ID: 3P8Z, 4CTJ, 4CTK, 4R05, 4R8S, 5CUQ, 5EIW, 8BCR, 5JJR, and 5JJS) [34–41], C-terminal NS5; RNA polymerase (PDB ID: 5F3T, 5F3Z, 5F41, 5I3P, 5I3Q, 6IZX, 6IZZ, 6XD0, and 6XD1) [41–44] , NS2B-NS3, protease (PDB ID: 6M9P, 3U1J active site, 3U1J allosteric binding site, 4M9K, 4M9M, and 4M9T) [45,46], and E envelope glycoprotein (PDB 1OAN and 1OKE) [47] as previously described in [48]. Before incorporating the coumarin ligands, the removal of solvent molecules and co-crystallized ligands was undertaken in each protein structure. A sphere, adequately sized to encompass the binding cavity, was centered on the binding site of each protein structure. Utilizing standard protonation states for neutral pH and charges derived from templates employed by the Molegro Virtual Docker program, each protein's configuration was established. Spartan ’18 for Windows (version 1.4.4, Wavefunction Inc., Irvine, California, USA) was employed for constructing each structure. Conformational analysis of the coumarin ligands was conducted using the MMFF (Merck Molecular Force Field) [49]. The docking process utilized flexible ligand models, while rigid model protein structures were employed. Each docking run was set with 1500 iterations, a maximum population size of 50, and 300 runs per ligand. The RMSD threshold for multiple poses was defined at 1.00 Å. Ligand poses were sorted based on the calculated "re-rank" score. To address potential bias towards high molecular weight compounds [50–55], a normalization scheme was incorporated:

$$DS_{norm} = 6.6 \times E_{dock}/MW^{⅓}$$

In this context, DS_{norm} represents the normalized docking score, E_{dock} corresponds to the MolDock "re-rank" score, MW denotes molecular weight, and 6.6 serves as a scaling constant intended to align the average DS_{norm} values with those of E_{dock}[56].

Molecular Dynamics (MD) Simulation

The examination of temporal dynamics in molecular systems can be conducted using molecular dynamics (MD) simulation, a computational method that employs Newton's equations of motion. In this investigation, four docked complexes (ligands 6, 10, 15, and 20, which represented as SH, RH, MG and WL) underwent MD simulations lasting 100 nanoseconds using the Schrodinger program and the Desmond 2019-4 package [57]. The purpose was to evaluate the stability of receptors and their interactions with ligands. Each system underwent three identical parameterized simulations within a cubic space filled with water, modeled using the TIP3P equation during a 100 ns MD simulation. The ligands SH, RH, MG and WL contributed 21231, 21222, 21228, and 21207 water molecules, respectively, to the complex system. A 10 Å buffer distance separated complex atoms from the box's edge for orthorhombic simulation. After introducing the appropriate counter-ion, a 0.15 M NaCl solution maintained the isosmotic state of the simulation box. Following a reduction in energy consumption, the complex underwent a developmental run in the NPT ensemble class, with the trajectory recorded at 300 K and 1,013 Bar, capturing 1000 frames. Additionally, the Desmond Package toolkit, inclusive of a Simulation Interaction Diagram (SID), was employed to explore precise interactions between the protein and ligands. Analysis of Root Mean Square Deviation (RMSD) and Root Mean Square Fluctuation (RMSF) plots, along with protein-ligand interaction profiles, demonstrated the stability of the ligand for both the protein and the ligand-bound protein.

Binding Free Energy Calculation Using MM-GBSA

The evaluation of binding free energies in reference complexes and Dengue Virus Envelope Glycoprotein-ligand combinations was carried out using the molecular mechanics method to assess complex stability. The calculation utilized the molecular mechanics generalized Born surface area (MM/GBSA) approach to determine the binding free energy within protein-ligand complexes. This specific quantum mechanics calculation aims to reduce the occurrence of false-positive results in molecular docking experiments. The Prime MM/GBSA module in the Schrödinger suite was employed to examine the impact of interactions on the stability of ligand-protein associations. For the MM-GBSA calculations, the Desmond trajectory file was divided into discrete snapshots, and Schrödinger's thermal mmgbsa.py Python script was then used to compute the mean and standard deviation of the projected binding energy over the entire 100 ns duration. The entire process can be represented by the following equation:

$$\Delta G_{bind} = \Delta E_{MM} + \Delta G_{solv} + \Delta G_{SA}$$

$$\Delta E_{MM} = E_{(complex)} - E_{(ligand)} - E_{(protein)}$$

In this context, ΔE_{MM} represents the disparity in minimal energies between the relevant entities, while ΔG_{solv} indicates the variation in total solvation energies encompassing both ligands and proteins and the GBSA solvation energy of the complex. The discrepancy in surface energies between the complex and the aggregate surface energies of the protein and ligand is referred to as ΔG_{SA}.

Lipinski’s Rule and ADMET Prediction

The Lipinski's rule parameters were computed for the four molecules exhibiting the highest docking affinity through the utilization of the Swissadmet server [58]. The violation of multiple parameters among these molecules may signify potential challenges pertaining to bioavailability, thereby elevating the risk of their failure to manifest drug-like characteristics [59]. In addition to this, we employed the pkCSM web server [60] to prognosticate the ADMET properties—comprising Absorption, Distribution, Metabolism, and Excretion—

of the aforementioned quartet of molecules [61]. This multifaceted approach aids in a comprehensive evaluation of the molecular characteristics, thereby enhancing our understanding of their potential pharmacological utility.

Global and Local Reactivity Descriptors by DFT and Electrostatic Potential Maps

To ascertain the optimal molecular geometry of the coumarins investigated in the present study, a systematic conformational search was executed using the Hyperchem software [62]. Subsequently, the most stable structure, characterized by minimal energy, underwent a comprehensive geometry optimization within an aqueous environment. This optimization procedure was conducted utilizing the B3LYP/6-31+G(d,p) level of theory, incorporating the Polarizable Continuum Model (PCM) solvation model to mimic the aqueous phase conditions. To verify the stability of the optimized structure, vibrational frequencies were meticulously assessed, ensuring that the structure corresponds to a minimum on the energy potential surface. All computational analyses were executed employing the Gaussian 09 software [63], and the outcomes were visualized using the GaussView version 3.09 packages [64]. This rigorous computational protocol was employed to elucidate and refine the molecular architecture of the coumarin compounds under investigation, providing a robust foundation for subsequent analyses and interpretations in the context of their chemical and physical properties.

RESULTS AND DISCUSSION

Docking Studies

Molecular docking of 20 coumarin ligands with relevant dengue virus protein targets (NS3 helicase, NS5 RNA methyl transferase, NS5 RNA polymerase, NS2B-NS3 protease, and E envelope glycoprotein) was carried out using the Molegro Virtual Docker program. The lowest-energy docking scores are summarized in **Table 1**. Docking scores for each of the coumarin ligands with each PDB protein structure are compiled in Supplementary **Table S1**.

Table 1: Normalized docking scores (DS_{norm}, kJ/mol) for coumarin ligands with dengue virus protein targets.

No.	Coumarin Ligand	NS3 Helicase	NS5 RNA Methyl transferase	NS5RNA Polymerase	NS2B-NS3 Protease	Envelope glycoprotein
1	6,8-di-*t*-butylcoumarin	–94.6	–92.6	–103.7	–79.7	–106.2
2	6-*t*-octylcoumarin	–98.8	–97.8	–90.0	–89.8	–106.8
3	(*R*)-6-hydroxy-7-(5-hydroxy-3,7-dimethyl-2,6-octadienyloxy)coumarin	–115.8	–108.6	–101.0	–104.7	–126.8
4	(*R*)-acenocoumarol	–107.7	–100.8	–96.6	–92.2	–108.5
5	(*R*)-warfarin	–97.8	–93.7	–93.4	–89.7	–106.1
6	(*S*)-6-hydroxy-7-(5-hydroxy-3,7-dimethyl-2,6-octadienyloxy)coumarin {SH}	–106.0	–103.8	–97.6	–103.6	–129.8
7	(*S*)-acenocoumarol	–108.1	–94.7	–96.0	–91.3	–104.4
8	(*S*)-warfarin	–97.8	–90.2	–88.7	–88.1	–113.1
9	6,7-diacetylesculetin	–93.0	–95.5	–95.6	–80.5	–102.6
10	6-hydroxy-7-(7-hydroxy-3,7-dimethyl-2,5-octadienyloxy)coumarin {RH}	–106.9	–110.5	–100.5	–104.1	–122.3
11	7-prenyloxycoumarin	–96.2	–95.9	–90.4	–94.1	–107.0
12	coumestrol	–93.7	–91.5	–96.3	–93.9	–104.7
13	esculetin	–84.3	–87.7	–86.6	–80.8	–95.8
14	esculin	–99.8	–91.9	–95.4	–98.2	–99.7
15	medicagol {MG}	–95.4	–90.7	–94.2	–88.7	–108.7
16	*neo*-tanshinlactone	–90.5	–90.0	–99.9	–77.8	–104.6
17	plicadin	–95.5	–94.0	–89.7	–89.1	–92.3
18	prenyletin	–96.4	–93.1	–92.4	–89.6	–102.5
19	umbelliferone	–84.6	–83.2	–81.1	–77.1	–89.7
20	wedelolactone {WL}	–94.4	–96.5	–98.3	–93.4	–111.2

Dengue virus NS3 helicase shows ATP hydrolysis and RNA duplex unwinding activities and is essential for viral replication [48]. (*R*)-6-Hydroxy-7-(5-hydroxy-3,7-dimethyl-2,6-octadienyloxy)coumarin showed the best docking properties with NS3 helicase (DS_{norm} = –115.8 kJ/mol). The lowest-energy docking pose of the ligand was within the RNA binding site of the enzyme. Key intermolecular contacts between the ligand and the protein residues were HIS 287 (van der Waals), THR 289 (van der Waals), SER 453 (van der Waals), GLU 412 (van der Waals), THR 450 (hydrogen bonding), PRO 319 (van der Waals), Ser452 (hydrogen bonding), and THR 317 (hydrogen bonding) **(Figure 2).**

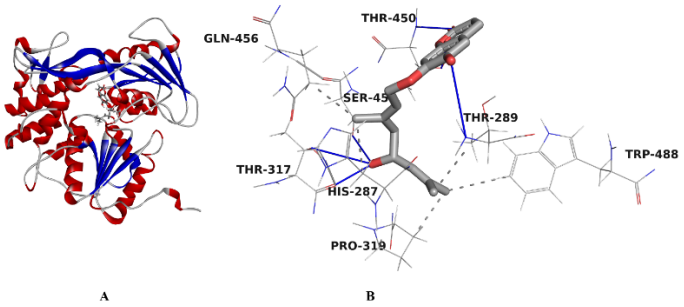

Figure 2: Lowest-energy docked pose of (*R*)-6-hydroxy-7-(5-hydroxy-3,7-dimethyl-2,6-octadienyloxy) coumarin with dengue virus NS3 helicase (PDB 2BMF). **B:** Key intermolecular interactions between the coumarin ligand and the protein residues; Hydrogen-bonding interactions are shown with dashed lines.

Dengue virus methyl transferase, located on the *N*-terminus of NS5, catalyzes the *N*-7 and 2′-*O* methylations of the viral RNA cap, which are necessary for the formation of the mature RNA cap structure [48]. The lowest-energy docking coumarin ligand was 6-hydroxy-7-(7-hydroxy-3,7-dimethyl-2,5-octadienyloxy) coumarin with a normalized docking score of –110.5 kJ/mol. The methyl transferase uses S-adenosylmethionine (SAM) as the methylating cofactor, and the coumarin ligand binds to the SAM binding site. Key interactions between the ligand and the protein include the residues ASP 146 (hydrogen bonding), GLY 83 (hydrogen bonding), LYS 105 (van der Waals), GLY 81 (van der Waals), CYS 82 (van der Waals), ARG 84 (hydrogen bonding), GLU 111 (van der Waals), ASP 131 (hydrogen bonding), VAL 132 (hydrogen bonding), GLY 86 (hydrogen bonding), GLY 85 (hydrogen bonding), and SER 56 (hydrogen bonding) **(Figure 3).**

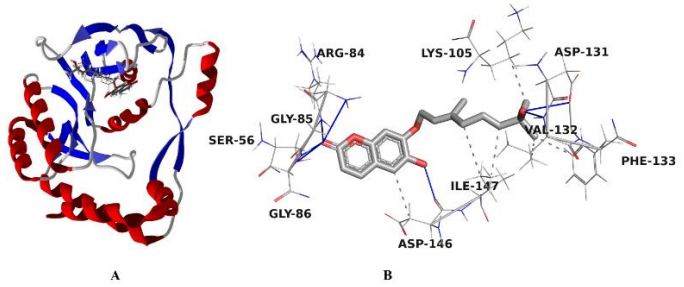

Figure 3: Lowest-energy docked pose of 6-hydroxy-7-(7-hydroxy-3,7-dimethyl-2,5-octadienyloxy)coumarin with NS5 RNA methyl transferase (PDB 8BCR). **A:** Ribbon structure of the protein; the coumarin ligand is shown as a thick stick figure and the *S*-adenosylmethionine co-crystallized ligand is shown as a thin stick figure. **B:** Key intermolecular interactions between the coumarin ligand and the protein residues; hydrogen bonds are shown as dashed lines.

Dengue virus NS5 RNA polymerase is an essential enzyme for viral replication. Furthermore, there are no similar enzymes found in host organisms [48]. The coumarin with the best docking score was 6,8-di-*t*-butylcoumarin (DS_{norm} = –103.7 kJ/mol), followed by (*R*)-6-hydroxy-7-(5-hydroxy-3,7-dimethyl-2,6-octadienyloxy)coumarin (DS_{norm} = –101.0 kJ/mol) and 6-hydroxy-7-(7-hydroxy-3,7-dimethyl-2,5-octadienyloxy)coumarin (DS_{norm} = –100.5 kJ/mol) (Table X). The coumarin ligands bind to the enzyme at the RNA template tunnel **(Figure 4)**. Important interactions of 6,8-di-*t*-butylcoumarin in the binding site were PHE 464 (van der Waals), SER 470 (van der Waals), TRP 474 (face-to-face π-π), ARG 471 (van der Waals), GLY 465 (van der Waals), and SER 420 (van der Waals) **(Figure 4B)**.

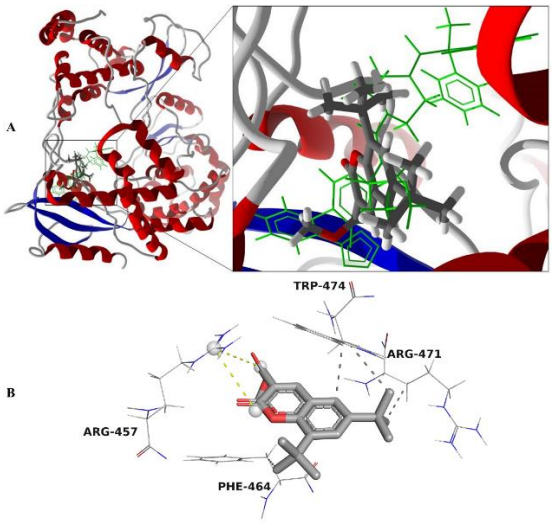

Figure 4: Lowest-energy docked pose of 6,8-di-*t*-butylcoumarin with dengue virus NS5 RNA polymerase (PDB 6XD1). **A:** Ribbon structure, the 6,8-di-*t*-butylcoumarin ligand is shown as a stick figure, the co-crystallized inhibitor [(2*R*)-4-(butyl{[2′-(1*H*-tetrazol-5-yl)[1,1′-biphenyl]-4-yl]methyl}carbamoyl)-1-(2,2-diphenylpropanoyl)piperazine-2-carboxylic acid)] is shown as a green wire figure. **B:** Key intermolecular contacts between 6,8-di-*t*-butylcoumarin and NS5 RNA polymerase.

The dengue virus NS2B-NS3 protease is a trypsin-like serine protease. The enzyme cleaves the dengue polyprotein into individual proteins that are necessary for the replication of the virus [48]. Both (*R*)- and (*S*)-6-hydroxy-7-(5-hydroxy-3,7-dimethyl-2,6-octadienyloxy) coumarin as well as 6-hydroxy-7-(7-hydroxy-3,7-dimethyl-2,5-octadienyloxy) coumarin showed good docking scores (DS_{norm} = –104.7, –103.6, and –104.1 kJ/mol, respectively) compared to the other coumarin ligands (DS_{norm} > –100 kJ/mol). These coumarin ligands docked preferentially to the allosteric binding site of the enzyme, surrounded by the amino acid residues LYS1074, ASN 1167, TRP 1089, ILE 1165, THR 1120, and ILE 1123 **(Figure 5)**.

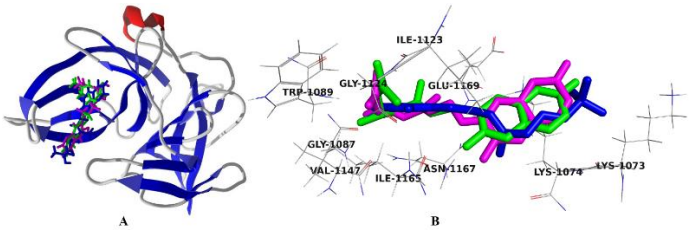

Figure 5: Lowest-energy docked poses of (*R*)-6-hydroxy-7-(5-hydroxy-3,7-dimethyl-2,6-octadienyloxy)coumarin (magenta), (*S*)-6-hydroxy-7-(5-hydroxy-3,7-dimethyl-2,6-octadienyloxy)coumarin (green), and 6-hydroxy-7-(7-hydroxy-3,7-dimethyl-2,5-octadienyloxy)coumarin (blue) in the allosteric binding site of dengue virus NS2B-NS3 protease (PDB 4M9T). **A:** Ribbon structure of the protein with the three coumarin ligands. **B:** Key residues in the allosteric binding site

The dengue virus E envelope glycoprotein mediates the binding of the virus to the host cell surface receptors. There is a small hydrophobic channel in the envelope protein that has been identified as a target for small-molecule virus inhibitors **(Figure 6A)** [48]. This protein target is clearly the best target for the coumarin compounds, which show docking energies near or greater than 200 kJ/mol. The coumarin ligands with the best docking scores with dengue virus envelope protein were (*R*)- and (*S*)-6-hydroxy-7-(5-hydroxy-3,7-dimethyl-2,6-octadienyloxy) coumarin (DS_{norm} = –126.8 and –129.8 kJ/mol, respectively). The important interactions of the (*S*)-6-hydroxy-7-(5-hydroxy-3,7-dimethyl-2,6-octadienyloxy) coumarin ligand with the protein were GLN 271B (hydrogen bonding), LYS 241A (hydrogen bonding), LYS 247A (van der Waals), HIS 244A (hydrogen bonding), LYS 204B (van der Waals), PRO 243A (van der Waals), ASP 249A (hydrogen bonding), and ASP 203B (hydrogen bonding) **(Figure 6B)**.

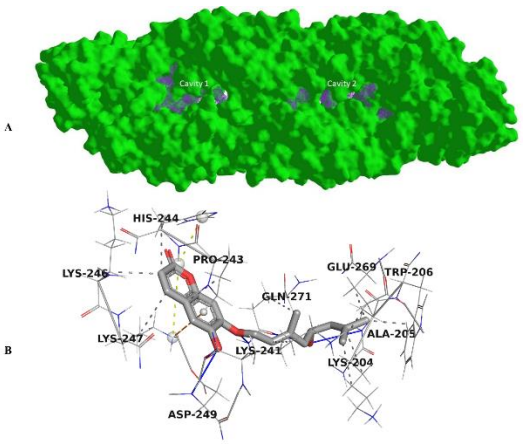

Figure 6: Dengue virus envelope glycoprotein (PDB 1OAN). **A:** Surface structure of the envelope protein; the cavities are shown in magenta. **B:** Lowest-energy docked pose of (*S*)-6-hydroxy-7-(5-hydroxy-3,7-dimethyl-2,6-octadienyloxy)coumarin in cavity 2; hydrogen bonds are shown as blue dashed lines.

MD Simulations

To explore the stability of complexes and binding interactions within the active pocket, molecular dynamics (MD) simulations were conducted over a duration of 100 nanoseconds. The Desmond program (version 2019-4, Schrödinger) was utilized to assess the stability of four distinct ligand-protein docking complexes, each featuring SH, RH, MG and WL ligands. The conformational landscapes of these complexes were investigated under specific conditions such as temperature and pressure. The MD simulation trajectory, corresponding to the simulation time, revealed the dynamic behavior of the docked complexes involving the Dengue Virus Envelope Glycoprotein and ligands. Various intermolecular interactions, including hydrogen bonds, were observed between ligands and amino acid residues within the active site of the Envelope Glycoprotein. Diverse noncovalent contact interactions, such as salt bridges, hydrophobic interactions, and both positive and negative polar contacts, were identified.

The stability of the docked Envelope Glycoprotein complexes was further examined by analysing hydrophobic, ionic, hydrogen bonding, and water-bridging interactions between ligands and proteins, as illustrated in **Figures 7 and 8**. A specific amino acid residue within one of the Glycoprotein's selective pockets exhibited favourable interactions with all docking ligands. Notably, the docked 1OAN ligands contributed to various hydrophobic, ionic, hydrogen bonding, and water-bridging interactions. Selected coumarin ligands were specifically evaluated for their ability to form strong hydrogen bond interactions with key residues in the Envelope Glycoprotein's selective pocket [65]. Analysis of intermolecular interaction maps derived from the simulation revealed that coumarin ligands-maintained interactions with specific residues throughout the simulation duration. This observation highlights the significance of the ligands' capability to sustain interactions over time. In conclusion, the results indicated that coumarin ligands consistently exhibited a binding orientation within the selective pocket of the Envelope Glycoprotein.

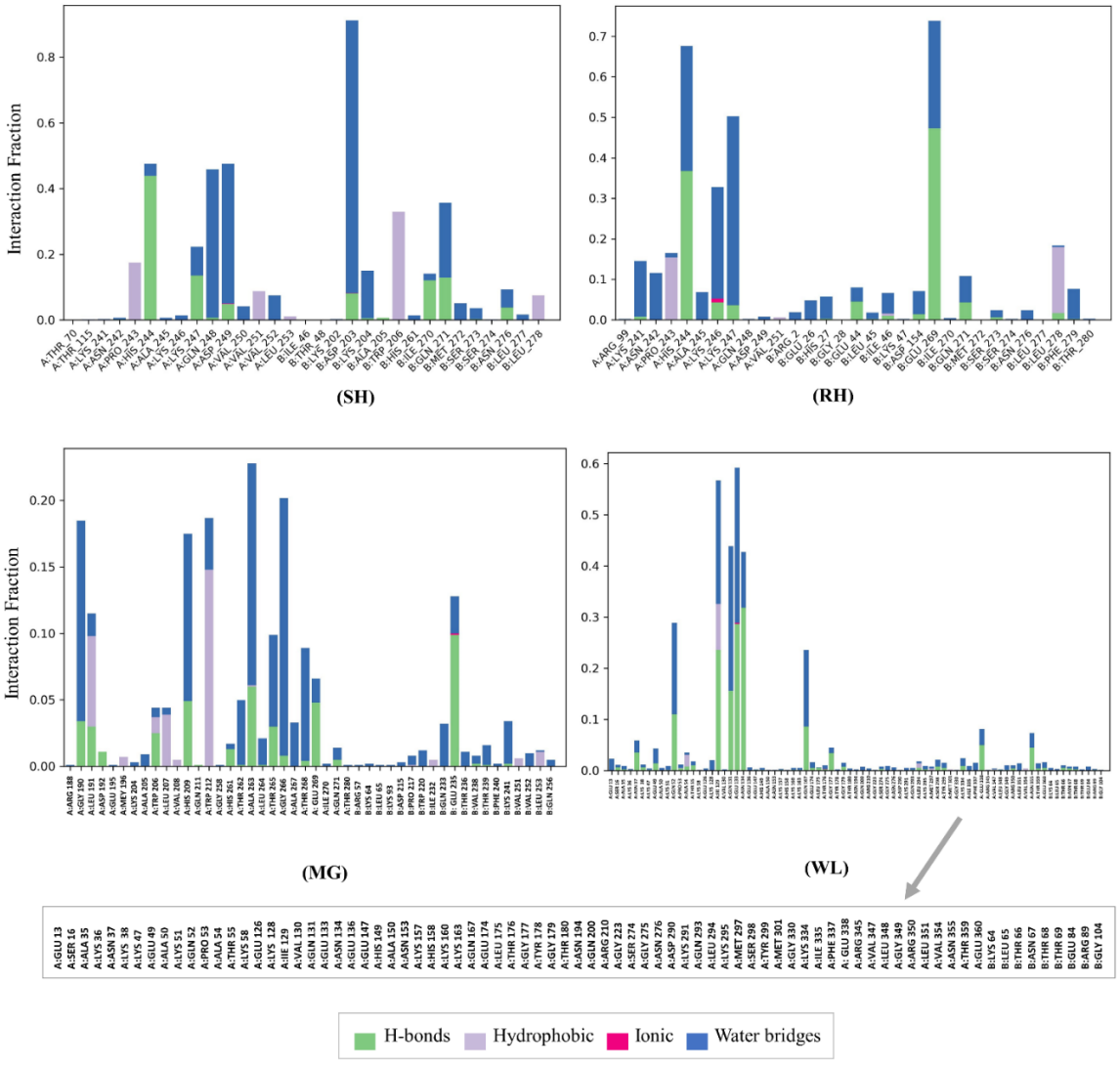

Figure 7: Protein-ligand contact plot (Selected ligands with 1OAN)

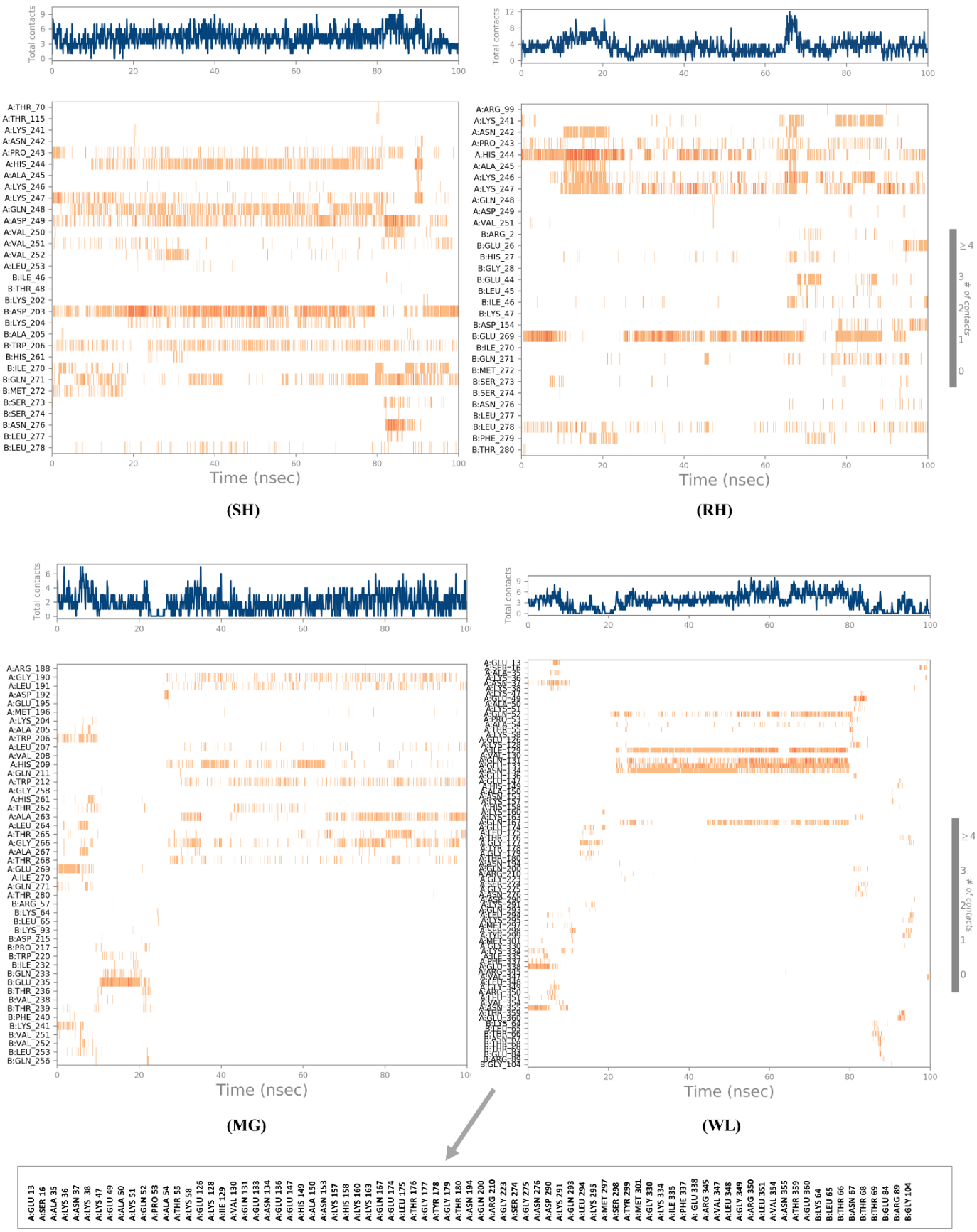

Figure 8: A timeline depiction of the interactions and connections (Selected ligands with 1OAN): The upper panel illustrates the total count of distinct contacts established by the protein with the ligand throughout the trajectory. In the lower panel, the interacting residues with the ligand are delineated for each frame. Certain residues engage in multiple specific interactions with the ligand, denoted by a deeper shade of orange as per the scale provided on the right side of the graph.

The quantification of the MD response involves assessing the Root Mean Square Deviation (RMSD) values of the protein's Cα backbone and the ligand data trajectories. Consequently, the stability of both the protein and the ligand-protein complex was analysed employing the RMSD methodology. The RMSD approach allows for the identification of ligands with a higher likelihood of binding to specific protein binding pockets. In assessing the impact of chemicals on the conformational stability of 1OAN throughout simulations, a comparison was made between the RMSD values of Cα atoms for the four complexes and their initial structures.

The outcomes are graphically presented in **Figure 9**, showcasing the variation over simulation time. Over the 100 ns simulation period, the coumarin ligands displayed a structural alteration of less than 3.5 Å. Specifically, the selected ligands exhibited remarkable stability between 58 and 100 ns, with deviations remaining below 4.8 Å. Notably, compound wedelolactone {WL} exhibited a higher RMSD value at the 35 ns mark, followed by a consistent deviation from 58 ns onwards. This suggests that, during the simulation, the ligands underwent significant dispersion away from the binding site of the Envelope Glycoprotein.

The coumarin compounds (SH = 3.2 Å, RH = 3.4 Å, MG = 0.4 Å, and WL = 1.1 Å) demonstrated maximum permissible deviation and equilibrium throughout the simulation model. Consequently, it was observed that the selective pocket of the Envelope Glycoprotein exhibited notably greater stability with the coumarin bioactive chemicals medicagol {MG} and wedelolactone {WL}. **Figure 10** illustrates that, within the active site, components 6-hydroxy-7-(7-hydroxy-3,7-dimethyl-2,5-octadienyloxy)coumarin {RH} and (S)-6-hydroxy-7-(5-hydroxy-3,7-dimethyl-2,6-octadienyloxy)coumarin {SH} underwent an approximate 3.5 Å movement relative to their reference confirmation before reaching equilibrium before 70 ns. In contrast, the RMSD of ligands 15 and 20 remained constant throughout the simulation period.

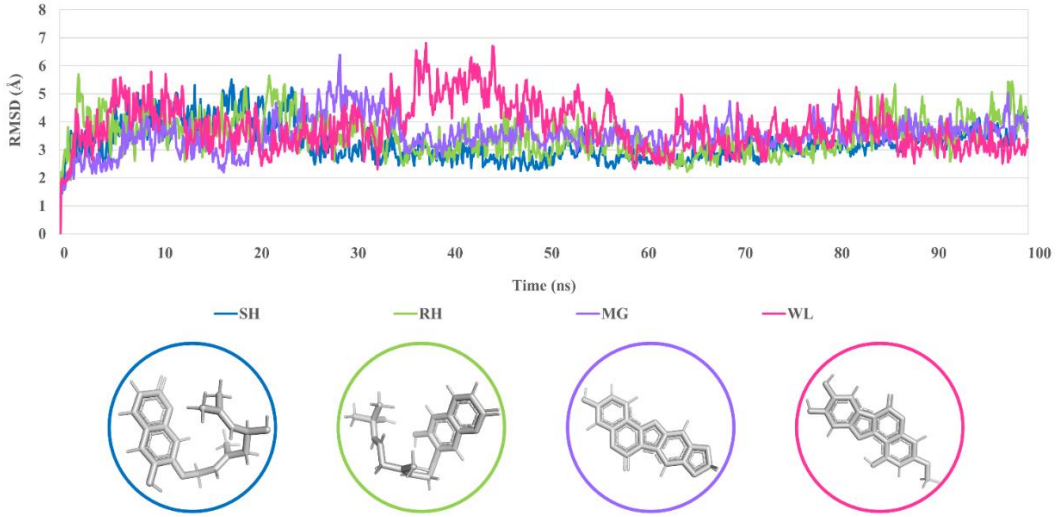

Figure 9: RMSD plot for Cα atoms (Å) with the selected compounds

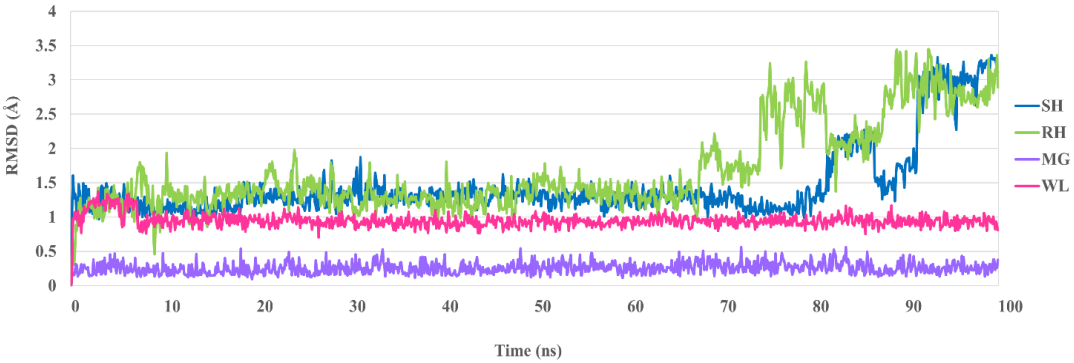

Figure 10: RMSD plot for ligand atoms (Å) in the presence of the chosen ligands

Figure 11 displays the results of the RMSF analysis carried out on the 100-nanosecond simulation trajectories of the Envelope Glycoprotein and the evaluated ligands within their respective complexes. RMSF is utilized as a method to quantify the degree to which an element or a set of elements has deviated from its reference structure, enabling the examination of time-dependent motions within a structure. While RMSD is conventionally used to assess whether a structure remains stable or deviates from its initial coordinate system during a simulation, proteins typically undergo more rapid evolution near their N- and C-terminal tails. In contrast, certain secondary structures, such as alpha helices and beta strands, tend to be more rigid and exhibit less variability than unstructured segments and loop sections [66].

The analysis disclosed a comparable range of variations (RMSF: 1.0 - 4.6 Å) for the C-terminal amino acid residues and the loop region of the Envelope Glycoprotein throughout the 100-nanosecond simulation of the docked complexes with the selected ligands. Consequently, the computed results suggest that the selected ligands exhibit enhanced stability within the designated active site of 1OAN compared to the reference ligand during the 100-nanosecond MD simulation. The highest RMSF value for complex {SH} was observed at GLY 330, measuring 4.267 Å. In contrast, the RMSF of the 1OAN-wedelolactone {WL} complex displayed greater stability, experiencing a smaller decline. Residues ASP 329 and LYS 344 exhibited the highest RMSFs, measuring 4.307 and 4.483 angstroms, respectively. While the complex 1OAN-6-hydroxy-7-(7-hydroxy-3,7-dimethyl-2,5-octadienyloxy)coumarin {RH} demonstrated effective stability during the MD simulation, no significant variations were noted. The highest RMSF value for the medicagol complex {MG} occurred at THR 155, measuring 4.605 Å.

The analysis disclosed a comparable range of variations (RMSF: 1.0 - 4.6 Å) for the C-terminal amino acid residues and the loop region of the Envelope Glycoprotein throughout the 100-nanosecond simulation of the docked complexes with the selected ligands. Consequently, the computed results suggest

that the selected ligands exhibit enhanced stability within the designated active site of 1OAN compared to the reference ligand during the 100-nanosecond MD simulation. The highest RMSF value for complex {SH} was observed at GLY 330, measuring 4.267 Å. In contrast, the RMSF of the 1OAN-wedelolactone {WL} complex displayed greater stability, experiencing a smaller decline. Residues ASP 329 and LYS 344 exhibited the highest RMSFs, measuring 4.307 and 4.483 angstroms, respectively. While the complex 1OAN-6-hydroxy-7-(7-hydroxy-3,7-dimethyl-2,5-octadienyloxy)coumarin {RH} demonstrated effective stability during the MD simulation, no significant variations were noted. The highest RMSF value for the medicagol complex {MG} occurred at THR 155, measuring 4.605 Å.

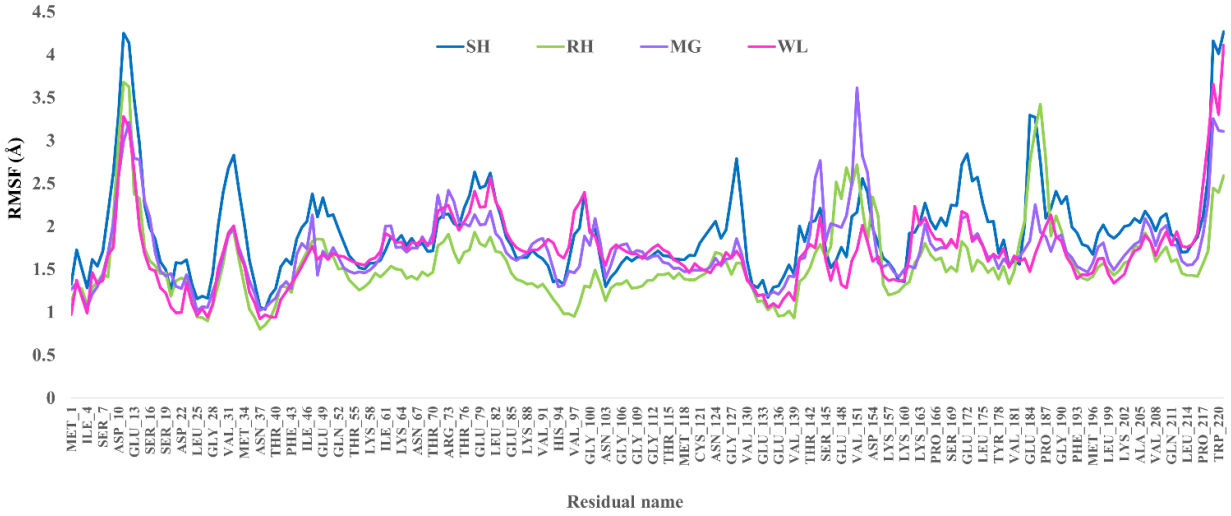

Figure 11: RMSF plot for or the Envelope Glycoprotein in conjunction with the chosen ligands

Prime MM-GBSA Calculation

The mean binding energy of a stabilized molecular dynamics trajectory was determined by analyzing two hundred frames at 50-picosecond intervals. The binding energy for each MD trajectory was computed using established formulas [67]. The Schrödinger's thermal mmgbsa.py Python script facilitated the calculation of the mean MM-GBSA binding energy. Furthermore, various energy components, including Coulombic (Coulomb), covalent binding energy (Covalent), hydrogen-bonding energy (H-bond), lipophilic energy (Lipo), generalized Born electrostatic solvation energy (Solv_GB), and van der Waals energy (vdW), were calculated using this application. The summarized data is presented in **Table 2**. Compounds ((S)-6-hydroxy-7-(5-hydroxy-3,7-dimethyl-2,6-octadienyloxy)coumarin) {SH} and (6-hydroxy-7-(7-hydroxy-3,7-dimethyl-2,5-octadienyloxy)coumarin) {RH} exhibited strong van der Waals interactions, high binding, and lipophilic energy. Compound wedelolactone {WL} displayed a higher Coulombic binding energy than ligand MG, despite having similar Solv_GB energy. In contrast, medicagol compound {MG} exhibited lower Coulombic energy. Notably, the Coulombic energy of compound RH was found to be favorable compared to other ligands.

Table 2. Calculation outcomes of MM-GBSA for the chosen ligands binding within the active site of 1OAN

Compound	ΔG Binding	Coulomb	Covalent	H-bond	Lipo	Solv_GB	vdW
SH	-66.704	-70.273	4.709	-0.639	-37.550	22.478	-48.674
RH	-81.799	-25.088	1.012	-0.567	-40.091	25.534	-43.599
MG	-54.911	-8.398	1.040	-0.363	-29.464	15.694	-33.422
WL	-47.485	-11.712	1.561	-0.524	-27.166	15.942	-25.586

Lipinski's Rule and ADME Prediction

In this study the four first compounds with the best affinity in the studied receptor have been selected. **Table 3** provides details of Lipinski's rule parameters, encompassing molecular weight, the count of rotatable bonds, the count of hydrogen bond acceptors, the count of hydrogen bond donors, and logP.

Compound		Property					Lipinski violations
		Log P	H-bond Acceptor	H-bond Donor	Rotatable bonds	Molecular weight g/mol	
	Rule	<4.15	≤10	<5	<10	≤500	≤1
N°	**Name**						
MG	Medicagol	1.87	6	1	0	296.23	0
WL	Wedelolactone	0.93	7	3	1	314.25	0
SH	(S)-6-hydroxy-7-(5-hydroxy-3,7-dimethyl-2,6-octadienyloxy)coumarin	2.10	5	2	6	330.37	0
RH	6-hydroxy-7-(7-hydroxy-3,7-dimethyl-2,5-octadienyloxy)coumarin	2.10	5	2	6	330.37	0

All the chosen compounds adhere to the criteria outlined in Lipinski's rule, without any violations. Consequently, all selected compounds demonstrate favourable bioavailability parameters. In this study, ADMET prediction was employed to assess the pharmacokinetic parameters of the top four compounds with the highest affinity, given their compliance with Lipinski's rule conditions (refer to **Table 4**). All chosen molecules exhibit low BBB permeability. The four molecules are fully absorbed, and other pharmacokinetic parameters, such as human intestinal absorption (HIA) and water solubility (log mol/L), meet acceptable standards.

Table 4. In silico ADMET properties of selected compounds.

			MG	WL	SH	RH
Property	**Model Name**	**Unit**	**Predicted Value**			
Absorption	Water solubility	Numeric (log mol/L)	-3.495	-3.419	-3.994	-3.923
	Caco2 permeability	Numeric (log Papp in 10^{-6} cm/s)	1.034	0.232	0.98	1.034
	Intestinal absorption (human)	Numeric (% Absorbed)	96.501	87.918	92.888	92.292
	Skin Permeability	Numeric (log Kp)	-2.696	-2.736	-3.139	-2.884
	P-glycoprotein substrate	Categorical (Yes/No)	No	Yes	Yes	Yes
	P-glycoprotein I inhibitor		No	No	Yes	Yes
	P-glycoprotein II inhibitor		No	No	No	No
Distribution	VDss (human)	Numeric (log L/kg)	0.182	-0.241	0.163	0.197
	Fraction unbound (human)	Numeric (Fu)	0.256	0.079	0.218	0.123
	BBB permeability	Numeric (log BB)	-0.697	-1.167	-0.52	-0.541
	CNS permeability	Numeric (log PS)	-2.016	-2.256	-2.277	-2.291
Metabolism	CYP2D6 substrate	Categorical (Yes/No)	No	No	No	No
	CYP3A4 substrate		Yes	No	No	Yes
	CYP1A2 inhibitior		Yes	Yes	Yes	Yes
	CYP2C19 inhibitior		Yes	No	Yes	Yes
	CYP2C9 inhibitior		Yes	Yes	Yes	Yes
	CYP2D6 inhibitior		No	No	No	No
	CYP3A4 inhibitior		Yes	No	No	No
Excretion	Total Clearance	Numeric (log ml/min/kg)	0.598	0.712	0.826	0.797
	Renal OCT2 substrate	Categorical (Yes/No)	No	No	No	Yes
Toxicity	AMES toxicity		Yes	Yes	No	Yes
	Max. tolerated dose (human)	Numeric (log mg/kg/day)	-0.159	0.619	0.349	0.502
	hERG I inhibitor	Categorical (Yes/No)	No	No	No	No
	hERG II inhibitor		No	Yes	No	No
	Oral Rat Acute Toxicity (LD50)	Numeric (mol/kg)	2.589	2.337	2.235	2.141
	Oral Rat Chronic Toxicity (LOAEL)	Numeric (log mg/kg_bw/day)	0.862	0.872	2.053	1.403
	Hepatotoxicity	Categorical (Yes/No)	No	No	No	No
	Skin Sensitisation		No	No	No	No
	T.Pyriformis toxicity	Numeric (log ug/L)	0.321	0.306	1.354	1.403
	Minnow toxicity	Numeric (log mM)	-0.162	0.655	-1.23	-0.993

Global and Local Reactivity Descriptors by DFT and Electrostatic Potential Maps

Reactivity analysis provides an understanding of how chemical compounds interact with biological receptors in the body, which is vital in the development of effective and safe drugs. Thus, in this work, the chemical reactivities of (R)-6-hydroxy-7-(5-hydroxy-3,7-dimethyl-2,6-octadienyloxy)coumarin {RH}, (S)-6-hydroxy-7-(5-hydroxy-3,7-dimethyl-2,6-octadienyloxy)coumarin {SH}, medicagol {MG}, and wedelolactone {WL}, were analyzed employing global and local reactivity descriptors evaluated at the B3LYP/6-31+G(d,p) level of theory. The global reactivity parameters evaluated were the electronic chemical potential (μ), the hardness (η), and the electrophilicity index (ω) [68,69].

$$\mu = \left(\frac{\partial E}{\partial N}\right)_{v(r)} = -\frac{1}{2}(I + A) \quad (1)$$

$$\eta = \left(\frac{\partial \mu}{\partial N}\right)_{v(r)} = \left(\frac{\partial^2 E}{\partial N^2}\right)_{v(r)} = (I - A) = (\varepsilon_L - \varepsilon_H) \quad (2)$$

$$\omega = \frac{\mu^2}{2\eta} \quad (3)$$

The energy, the number of electrons, and the external potential exerted by the nucleus are represented by E, N and v(r), respectively, in these equations. The electronic affinity is represented by A, and the ionization potential is denoted by I. μ allows measuring the ability to transfer electrons to another molecular system, while η indicates the polarizability or stability of the molecular system. On the other hand, ω measures the ability to accept electrons, a good nucleophile is suggested by low ω values, and a good electrophile is indicated by larger values. In Table 5 the reactivity parameters that describe the general chemical behaviour of the coumarins RH, SH, MG and WL are reported. Note that RH and SH exhibit similar reactivity parameter values. However, in comparison, MG and WL have a lower ability to transfer electrons because they exhibit a lower value of μ. Also, note that the ω values indicate that the nucleophilicity order is given by WL > MG > SH=RH. The last results suggest that in this group, WL and MG are more nucleophilic than SH and RH. However, RH and SH are more stable than WL and MG.

Table 5. Global reactivity descriptors for RH, SH, MG and WL at the B3LYP/6-31+G(d level of theory in the aqueous phase according to equations (1), (2) and (3).

Ligands {Abbriviation}	μ / eV	η / eV	ω / eV
6-hydroxy-7-(7-hydroxy-3,7-dimethyl-2,5-octadienyloxy)coumarin {SH}	4.11	3.84	2.20
(S)-6-hydroxy-7-(5-hydroxy-3,7-dimethyl-2,6-octadienyloxy)coumarin {RH}	4.11	3.84	2.20
Medicagol {MG}	3.88	3.52	2.14
Wedelolactone {WL}	3.88	3.60	2.09

In addition, to investigate the point distribution of the active sites for different types of attacks on the coumarins studied in the present work, the local reactivity was evaluated using the Fukui Function, $f(r)$:[70]

$$f(r) = \left(\frac{\partial \rho(r)}{\partial N}\right)_{v(r)} = \left(\frac{\partial \mu(r)}{\partial v(r)}\right) \quad (4)$$

where, $\rho(r)$ is the electron density. $f(r)$ in an atomic position can be evaluated by using the atomic charge approximation, as shown in equations (5), (6) and (7)[70].

$$f_j^-(r) = q_{j(N-1)} - q_{j(N)} \quad (5)$$

$$f_j^+(r) = q_{j(N)} - q_{j(N+1)} \quad (6)$$

$$f_j^0(r) = {}^1/_2\,(q_{j(N-1)} - q_{j(N+1)}) \quad (7)$$

where q_j is the atomic charge at the site $j_{ésimo}$ neutral (N)anionic $(N+1)$ or cationic $(N-1)$ of the chemical species. In this work, we used the Hirshfeld population [71], to evaluate the $f(r)$, through equations (5)-(7). For RH **(Figure 12)**, the most reactive sites to nucleophilic and electrophilic attacks were located at atoms 9C, 11C, and 15O, while for free radical attacks, the most reactive sites are at atoms 6C, 15O, and 17O. In the case of SH, atoms 9C, 11C, and 15O are sites susceptible to nucleophilic and free radical attacks. In the case of electrophilic attacks, 5C, 11C, and 15O turn out to be the most reactive sites. For nucleophilic and free radical attacks on medicagol , the most reactive sites are found at 3C, 9C, and 12O, while electrophilic attacks are expected at 16C, 18C, and 24O. In wendelolactone, 9C, 11C, and 12O are the most reactive sites for nucleophilic attacks, 9C, 10C, and 12O for free radical attacks, while electrophilic attacks occur at 12O, 22C, and 30O.

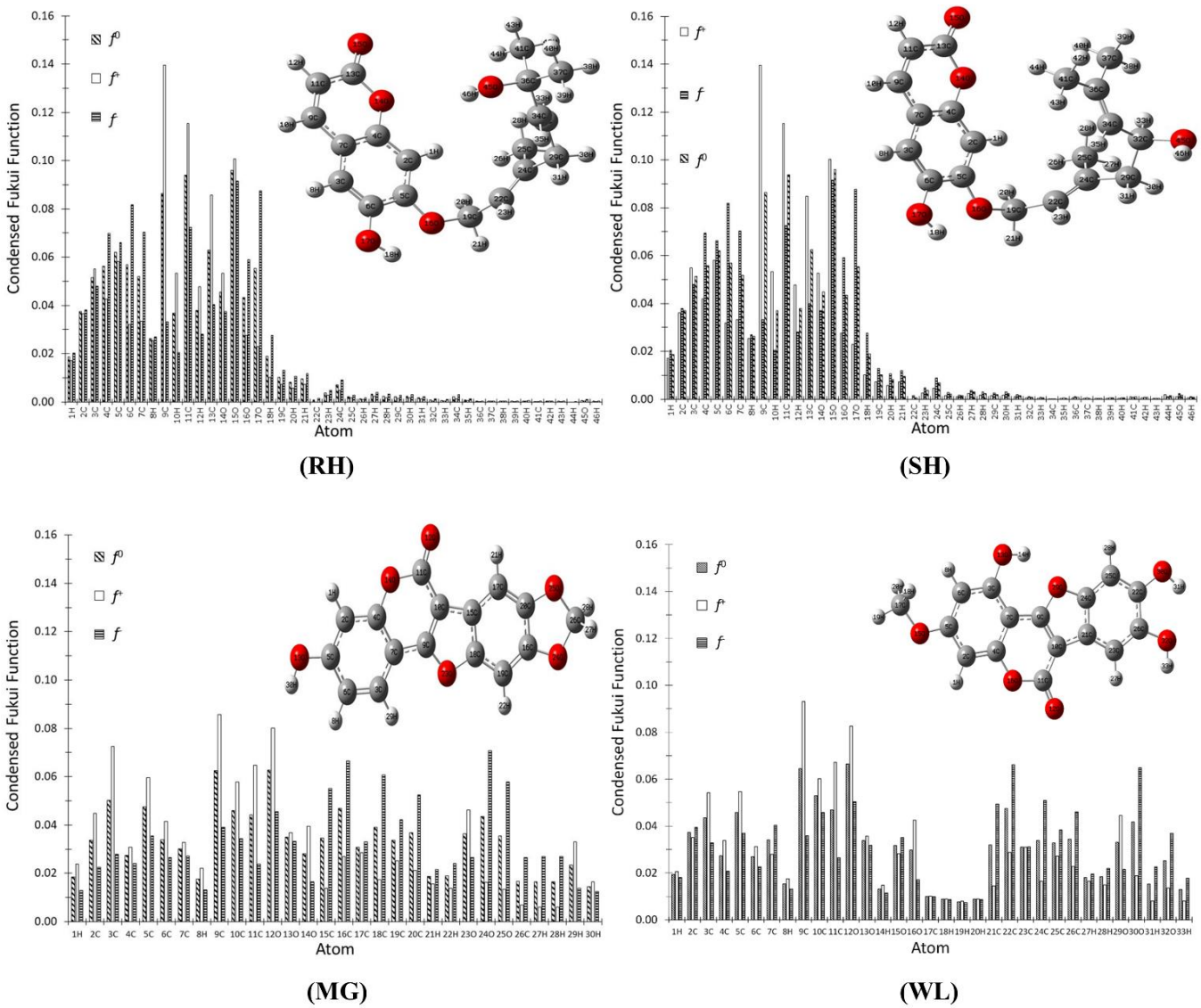

Figure 12. Calculations of the Fukui function RH, SH, MG, and WL are conducted, taking into account Hirshfeld charges for nucleophilic, electrophilic, and free radical attacks, as specified in equations (5-7).

It is also important to mention here that electrostatic potential maps (MEPs) allow us to visualize how positive and negative charges are distributed in a molecule. This is important since partially charged regions can influence the interaction of the molecule with other substances, facilitating or hindering the interaction of the molecule with other substances and favoring or inhibiting chemical reactions. Thus, regions of high electron density (negative charges) or low electron density (positive charges) on an electrostatic potential map indicate sites where electrostatic interactions, such as chemical bonds or intermolecular interactions, are more likely to occur. Thus, this kind of maps allows us to identify the nucleophilic and electrophilic sites on a compound [72]. In **Figure 13** is depicted the MEPs for RH, SH, MG, and WL. Note that in all cases, the zones with high electron density (red color) are on the oxygen atoms, suggesting that these sites may be more reactive to electrophilic reactions. The zones with low electron density (blue zones) are mainly located on the hydrogen atoms, which may interact with sites with high electron density.

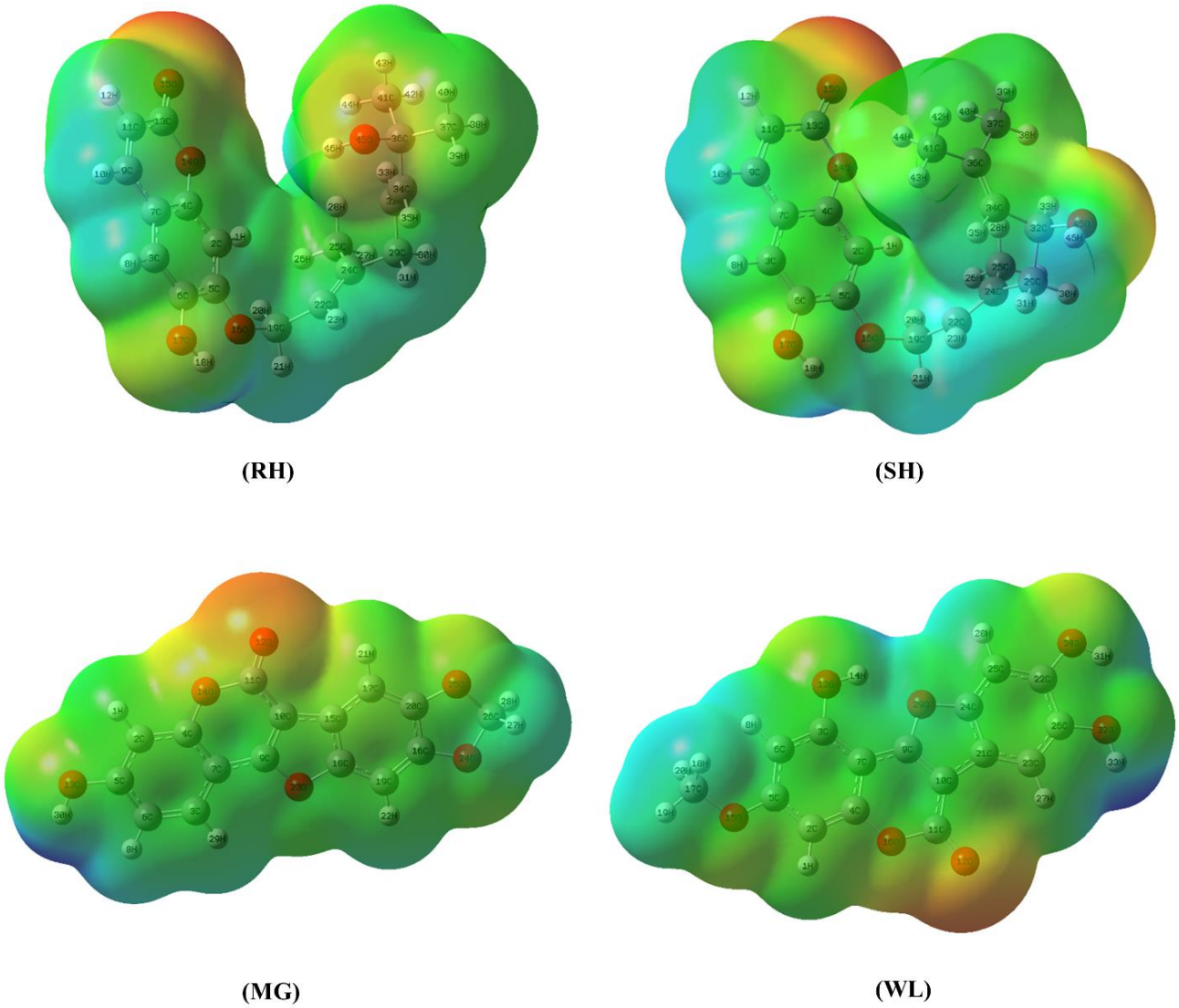

Figure 13. Maps of molecular electrostatic potential obtained at the B3LYP/6-31+G(d) level of theory onto a density isosurface of 0.002 e/u.a.3, for RH, SH, MG and WL

CONCLUSION

Dengue virus infections are a major public health issue in many countries, and there is no known effective antiviral treatment. One promising approach to fight Dengue is to use phytochemicals, specifically coumarins, as larvicide agents. Coumarins have a high degree of affinity for various dengue virus derivatives and protein targets. In this study, structural-based drug design was applied to create potential inhibitors for E envelop glycoprotein receptors to inhibit the enzyme's catalytic activity. ((S)-6-hydroxy-7-(5-hydroxy-3,7-dimethyl-2,6-octadienyloxy)coumarin, 6-hydroxy-7-(7-hydroxy-3,7-dimethyl-2,5-octadienyloxy)coumarin, wedelolactone, and medicagol showed increased binding energy and intermolecular interaction within the envelop glycoprotein pocket. These findings were based on a comprehensive computational analysis that included molecular docking and molecular dynamics simulations as well as MM/GBSA and quantum chemistry approaches, as well as drug-likeness assessment and in silico ADMET predictions. Furthermore, ligand atom mapping, the study also identified conformational alterations in conserved residues in docked complexes. In-silico investigations revealed that coumarin-derived ligands, especially hydroxylated, geranyloxy- substituted coumarins, preferentially bind to the dengue viral envelope protein. More *in-vitro* and *in vivo* studies are needed to understand the pharmacology and biological effects of these coumarin derived ligands, which will provide a better understanding of their antiviral activity.

ACKNOWLEDGEMENTS

The authors would like to thank Charmo University for their continued help and facilities in conducting this research. L.H.M.H. thankfully acknowledges the computer resources, technical expertise and support provided by the Laboratorio Nacional de Supercómputo del Sureste de México, CONACYT member of the network of National laboratories through the project No. 202203072N and to the Universidad Autónoma del Estado de Hidalgo.

FUNDING

This research did not receive any specific grant from funding agencies in the public, commercial, or not-for-profit sectors.

CONFLICT OF INTEREST

There are no conflicts of interest declared by the authors.

ETHICAL APPROVAL

This article does not contain any studied with human participants or animals performed by any of the authors.

AVAILABILITY OF DATA AND MATERIAL

All data generated during this study are included in supplementary information files.

CODE AVAILABILITY

Not applicable

AUTHORS' CONTRIBUTIONS

Conceptualization: HOR, GSM

Data curation: HOR, KRS

Software: DAH, GSM, WCV

Resources: WNS, KRS, LHM

Formal Analysis: LHM, AB

Investigation: AB, LGC

Methodology: LHM, LGC

Supervision: HOR, KRS

Visualization: WCV, WNS

Validation: DAH, GSM

Writing original draft: HOR, WNS

Writing review & editing: HOR, KRS

REFERENCES

1. O. J. Brady, P. W. Gething, S. Bhatt, J. P. Messina, J. S. Brownstein, A. G. Hoen, C. L. Moyes, A. W. Farlow, T. W. Scott, and S. I. Hay, (2012).
2. J. Whitehorn and C. P. Simmons, Vaccine **29**, 7221 (2011).
3. S. Mishra, A. Pandey, and S. Manvati, Heliyon **6**, (2020).
4. S. Bhatt, P. W. Gething, O. J. Brady, J. P. Messina, A. W. Farlow, C. L. Moyes, J. M. Drake, J. S. Brownstein, A. G. Hoen, and O. Sankoh, Nature **496**, 504 (2013).
5. J. D. Stanaway, D. S. Shepard, E. A. Undurraga, Y. A. Halasa, L. E. Coffeng, O. J. Brady, S. I. Hay, N. Bedi, I. M. Bensenor, and C. A. Castañeda-Orjuela, Lancet Infect. Dis. **16**, 712 (2016).
6. S. R. Mutheneni, A. P. Morse, C. Caminade, and S. M. Upadhyayula, Emerg. Microbes Infect. **6**, 1 (2017).
7. F. Meng, R. A. Badierah, H. A. Almehdar, E. M. Redwan, L. Kurgan, and V. N. Uversky, FEBS J. **282**, 3368 (2015).
8. V. D. Dwivedi, I. P. Tripathi, R. C. Tripathi, S. Bharadwaj, and S. K. Mishra, Brief. Funct. Genomics **16**, 217 (2017).
9. L. R. Souza, J. G. Colonna, J. M. Comodaro, and F. G. Naveca, BMC Bioinformatics **23**, 1 (2022).
10. H. K. H. Luk, X. Li, J. Fung, S. K. P. Lau, and P. C. Y. Woo, Infect. Genet. Evol. **71**, 21 (2019).
11. P. Bhatt, S. P. Sabeena, M. Varma, and G. Arunkumar, Curr. Microbiol. **78**, 17 (2021).
12. H. A. Imad, W. Phumratanaprapin, B. Phonrat, K. Chotivanich, P. Charunwatthana, S. Muangnoicharoen, S. Khusmith, T. Tantawichien, J. Phadungsombat, and E. Nakayama, Am. J. Trop. Med. Hyg. **102**, 943 (2020).
13. X. Pang, R. Zhang, and G. Cheng, Virol. Sin. **32**, 16 (2017).
14. K. N. Venugopala, V. Rashmi, and B. Odhav, Biomed Res. Int. **2013**, (2013).
15. A. Stefanachi, F. Leonetti, L. Pisani, M. Catto, and A. Carotti, Molecules **23**, 250 (2018).
16. S. D. Sarker and L. Nahar, Prog. Chem. Org. Nat. Prod. 106 241 (2017).
17. L. P. Jigar, *The Introduction of Coumarin* (Blue Rose Publishers, 2019).
18. N. H. Jadhav, S. S. Sakate, N. K. Rasal, D. R. Shinde, and R. A. Pawar, ACS Omega **4**, 8522 (2019).
19. M. Z. Hassan, H. Osman, M. A. Ali, and M. J. Ahsan, Eur. J. Med. Chem. **123**, 236 (2016).
20. R. W. DeSimone, K. S. Currie, S. A. Mitchell, J. W. Darrow, and D. A. Pippin, Comb. Chem. High Throughput Screen. **7**, 473 (2004).
21. D. Mathew and W.-L. Hsu, J. Funct. Foods **40**, 692 (2018).
22. J. Zhu and J. Jiang, Mol. Nutr. Food Res. **62**, 1701073 (2018).
23. U. Laila, M. Akram, M. A. Shariati, A. M. Hashmi, N. Akhtar, I. M. Tahir, A. O. Ghauri, N. Munir, M. Riaz, and N. Akhter, Clin. Exp. Pharmacol. Physiol. **46**, 1063 (2019).
24. D. Srikrishna, C. Godugu, and P. K. Dubey, Mini Rev. Med. Chem. **18**, 113 (2018).
25. E. Kudo, M. Taura, K. Matsuda, M. Shimamoto, R. Kariya, H. Goto, S. Hattori, S. Kimura, and S. Okada, Bioorg. Med. Chem. Lett. **23**, 606 (2013).
26. B. T. Dharmapalan, R. Biswas, S. Sankaran, B. Venkidasamy, M. Thiruvengadam, G. George, M. Rebezov, G. Zengin, M. Gallo, and D. Montesano, Viruses **14**, 2656 (2022).
27. G. M. Morris, R. Huey, W. Lindstrom, M. F. Sanner, R. K. Belew, D. S. Goodsell, and A. J. Olson, J. Comput. Chem. **30**, 2785 (2009).
28. D. B. Kitchen, H. Decornez, J. R. Furr, and J. Bajorath, Nat. Rev. Drug Discov. **3**, 935 (2004).
29. R. Thomsen and M. H. M. CHRISTENSEN, J. Med. Chem. 3315 (n.d.).
30. T. Xu, A. Sampath, A. Chao, D. Wen, M. Nanao, P. Chene, S. G. Vasudevan, and J. Lescar, J. Virol. **79**, 10278 (2005).
31. D. Luo, T. Xu, R. P. Watson, D. Scherer-Becker, A. Sampath, W. Jahnke, S. S. Yeong, C. H. Wang, S. P. Lim, A. Strongin, S. G. Vasudevan, and J. Lescar, EMBO J. **27**, 3209 (2008).
32. D. Luo, N. Wei, D. N. Doan, P. N. Paradkar, Y. Chong, A. D. Davidson, M. Kotaka, J. Lescar, and S. G. Vasudevan, J. Biol. Chem. **285**, 18817 (2010).
33. C. M. D. Swarbrick, C. Basavannacharya, K. W. K. Chan, S.-A. Chan, D. Singh, N. Wei, W. W. Phoo, D. Luo, J. Lescar, and S. G. Vasudevan, Nucleic Acids Res. **45**, 12904 (2017).
34. S. P. Lim, L. S. Sonntag, C. Noble, S. H. Nilar, R. H. Ng, G. Zou, P. Monaghan, K. Y. Chung, H. Dong, B. Liu, C. Bodenreider, G. Lee, M. Ding, W. L. Chan, G. Wang, Y. L. Jian, A. T. Chao, J. Lescar, Z. Yin, T. R. Vedananda, T. H. Keller, and P.-Y. Shi, J. Biol. Chem. **286**, 6233 (2011).
35. B. Coutard, E. Decroly, C. Li, A. Sharff, J. Lescar, G. Bricogne, and K. Barral, Antiviral Res. **106**, 61 (2014).
36. M. B. Brecher, Z. Li, J. Zhang, H. Chen, Q. Lin, B. Liu, and H. Li, Protein Sci. **24**, 117 (2015).
37. C. G. Noble, S.-H. Li, H. Dong, S. H. Chew, and P.-Y. Shi, Antiviral Res. **111**, 78 (2014).
38. M. Brecher, H. Chen, Z. Li, N. K. Banavali, S. A. Jones, J. Zhang, L. D. Kramer, and H. Li, ACS Infect. Dis. **1**, 340 (2015).
39. F. Benmansour, I. Trist, B. Coutard, E. Decroly, G. Querat, A. Brancale, and K. Barral, Eur. J. Med. Chem. **125**, 865 (2017).
40. M. Feracci, C. Eydoux, V. Fattorini, L. Lo Bello, P. Gauffre, B. Selisko, P. Sutto-Ortiz, A. Shannon, H. Xia, P.-Y. Shi, M. Noel, F. Debart, J.-J. Vasseur, S. Good, K. Lin, A. Moussa, J.-P. Sommadossi, A. Chazot, K. Alvarez, J.-C. Guillemot, E. Decroly, F. Ferron, and B. Canard, Antiviral Res. **212**, 105574 (2023).
41. S. P. Lim, C. G. Noble, C. C. Seh, T. S. Soh, A. El Sahili, G. K. Y. Chan, J. Lescar, R. Arora, T. Benson, S. Nilar, U. Manjunatha, K. F. Wan, H. Dong, X. Xie, P.-Y. Shi, and F. Yokokawa, PLoS Pathog. **12**, e1005737 (2016).
42. C. G. Noble, S. P. Lim, R. Arora, F. Yokokawa, S. Nilar, C. C. Seh, S. K. Wright, T. E. Benson, P. W. Smith, and P.-Y. Shi, J. Biol. Chem. **291**, 8541 (2016).
43. H. Shimizu, A. Saito, J. Mikuni, E. E. Nakayama, H. Koyama, T. Honma, M. Shirouzu, S.-I. Sekine, and T. Shioda, PLoS Negl. Trop. Dis. **13**, e0007894 (2019).
44. R. Arora, C. W. Liew, T. S. Soh, D. A. Otoo, C. C. Seh, K. Yue, S. Nilar, G. Wang, F. Yokokawa, C. G. Noble, Y. L. Chen, P.-Y. Shi, J. Lescar, T. M. Smith, T. E. Benson, and S. P. Lim, J. Virol. **94**, (2020).
45. C. G. Noble, C. C. Seh, A. T. Chao, and P. Y. Shi, J. Virol. **86**, 438 (2012).
46. M. Yildiz, S. Ghosh, J. A. Bell, W. Sherman, and J. A. Hardy, ACS Chem. Biol. **8**, 2744 (2013).
47. Y. Modis, S. Ogata, D. Clements, and S. C. Harrison, Proc. Natl. Acad. Sci. U. S. A. **100**, 6986 (2003).

48. C. N Powers and W. N Setzer, Comb. Chem. High Throughput Screen. **19**, 516 (2016).
49. T. A. Halgren, J. Comput. Chem. **17**, 490 (1996).
50. Y. Pan, N. Huang, S. Cho, and A. D. Mackerell, J. Chem. Inf. Comput. Sci. **43**, 267 (2003).
51. J. Yang and T. Shen, Proteins Struct. Funct. Bioinforma. **59**, 205 (2005).
52. N. Huang, A. Nagarsekar, G. Xia, J. Hayashi, and A. D. MacKerell, J. Med. Chem. **47**, 3502 (2004).
53. C. N. Hancock, A. Macias, E. K. Lee, S. Y. Yu, A. D. MacKerell, and P. Shapiro, J. Med. Chem. **48**, 4586 (2005).
54. C. Abad-Zapatero and J. T. Metz, Drug Discov. Today **10**, 464 (2005).
55. G. Carta, A. J. S. Knox, and D. G. Lloyd, J. Chem. Inf. Model. **47**, 1564 (2007).
56. M. Snow Setzer, K. G. Byler, I. V. Ogungbe, and W. N. Setzer, Sci. Pharm. **85**, 5 (2017).
57. S. Release, Maest. Interoperability Tools, Schrödinger, New York, NY (2017).
58. A. Daina, O. Michielin, and V. Zoete, Sci. Rep. **7**, 1 (2017).
59. Y. H. Zhao, M. H. Abraham, J. Le, A. Hersey, C. N. Luscombe, G. Beck, B. Sherborne, and I. Cooper, Pharm. Res. **19**, 1446 (2002).
60. D. E. V Pires, T. L. Blundell, and D. B. Ascher, J. Med. Chem. **58**, 4066 (2015).
61. C. B. Jalkute, S. H. Barage, M. J. Dhanavade, and K. D. Sonawane, Int. J. Pept. Res. Ther. **21**, 107 (2015).
62. Hypercube, (2007).
63. M. J. Frisch, G. W. Trucks, H. B. Schlegel, G. E. Scuseria, M. A. Robb, J. R. Cheeseman, G. Scalmani, V. Barone, B. Mennucci, G. A. Petersson, H. Nakatsuji, M. Caricato, X. Li, H. P. Hratchian, A. F. Izmaylov, J. Bloino, G. Zheng, J. L. Sonnenberg, M. Hada, M. Ehara, K. Toyota, R. Fukuda, J. Hasegawa, M. Ishida, T. Nakajima, Y. Honda, O. Kitao, H. Nakai, T. Vreven, J. A. Montgomery, J. E. Peralta, F. Ogliaro, M. Bearpark, J. J. Heyd, E. Brothers, K. N. Kudin, V. N. Staroverov, R. Kobayashi, J. Normand, K. Raghavachari, A. Rendell, J. C. Burant, S. S. Iyengar, J. Tomasi, M. Cossi, N. Rega, J. M. Millam, M. Klene, J. E. Knox, J. B. Cross, V. Bakken, C. Adamo, J. Jaramillo, R. Gomperts, R. E. Stratmann, O. Yazyev, A. J. Austin, R. Cammi, C. Pomelli, J. W. Ochterski, R. L. Martin, K. Morokuma, V. G. Zakrzewski, G. A. Voth, P. Salvador, J. J. Dannenberg, S. Dapprich, A. D. Daniels, Ö. Farkas, J. B. Foresman, J. V Ortiz, J. Cioslowski, and D. J. Fox, (2009).
64. D. R. D. K. T. A. M. JM, Gaussian Inc (2008).
65. H. O. Rasul, B. K. Aziz, D. D. Ghafour, and A. Kivrak, Mol. Divers. (2022).
66. L. Martínez, PLoS One **10**, e0119264 (2015).
67. R. Alnajjar, A. Mostafa, A. Kandeil, and A. A. Al-Karmalawy, Heliyon **6**, e05641 (2020).
68. P. Geerlings, F. De Proft, and W. Langenaeker, Chem. Rev. **103**, 1793 (2003).
69. P. K. Chattaraj, *Chemical Reactivity Theory : A Density Functional View*, First (CRC Press/Taylor & Francis, Boca Ratón, 2009).
70. R. G. Parr and W. Yang, J. Am. Chem. Soc. **106**, 4049 (1984).
71. F. L. Hirshfeld, Theor. Chim. Acta **44**, 129 (1977).
72. A. Kumar, C. G. Mohan, and P. C. Mishra, J. Mol. Struct. THEOCHEM **361**, 135 (1996).